GROUND DATA PROCESSING & PRODUCTION OF THE LEVEL 1 HIGH RESOLUTION MAPS

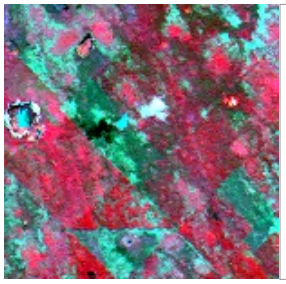

VALERI 2001

Laprida site
(grassland)

Philippe Rossello

February 2007

CONTENTS

1. Introduction

This report describes the production of high resolution, level 1, biophysical variable maps for the Laprida site in 2001 (see campaign report for more details about the site and the ground measurement campaign: annex or http://www.avignon.inra.fr/valeri). Level 1 map corresponds to the map derived from the determination of a transfer function between reflectance values of the SPOT image acquired during (or around) the ground campaign, and biophysical variable measurements (hemispherical images). For each Elementary Sampling Unit (ESU), the hemispherical images were processed using the CAN-EYE software (Version 4.2) developed at INRA-CSE. The derived biophysical variable maps are:

• four Leaf Area Index (LAI) are considered: effective LAI (LAIeff) and true LAI (LAItrue) derived from the measurement of the gap fraction as a function of the view zenith angle; effective LAI57 (LAI57eff) and true LAI57 (LAI57true) derived from the gap fraction at 57.5°, which is independent on leaf inclination. Effective LAI and effective LAI57 do not take into account clumping effect. LAItrue and LAI57true are derived using the method proposed by Lang and Xiang[1] (1986);

• cover fraction (fCover): it is the percentage of soil covered by vegetation. To improve the spatial sampling, fCover was computed over 0 to 10° zenith angle;

• fAPAR: it is the fraction of Absorbed Photosynthetically Active Radiation (PAR=400-700nm). fAPAR is defined either instantaneously (for a given solar position) or integrated all over the day. Following a study based on radiative transfer model simulations, it has been shown that the root mean square error between instantaneous fAPAR computed every 30 minutes and the daily fAPAR is the lowest for instantaneous fAPAR at 10h00 AM (solar time, RMSE = 0.021). Therefore, the derivation of fAPAR from CAN-EYE corresponds to the instantaneous black sky fAPAR at 10h00 AM.

The land cover is composed of grassland. The detailed description of the site is available in the campaign report[2]. The site is quite flat (altitude: ~ 200 m). It is approximately 3 x 3 km with coordinates described in Table 1:

	UTM 20, South WGS-84 (units = meters)		Geographic Lat/Lon WGS-84 (units = degrees)	
	Easting	Northing	Lat.	Lon.
Upper left corner	716279.6000	5904909.2000	-36.97709434	-60.57017039
Lower right corner	719319.6000	5901869.2000	-37.00376911	-60.53516172
Center	717799.6000	5903389.2000	-36.99043314	-60.55266911

Table 1. Description of the site coordinates.

The ground measurements were carried out from 2001/11/5 to 2001/11/8, while the high spatial resolution image (SPOT4, HRVIR2, resolution: 20 m) was acquired on 2001/11/3.

2. Available data

2.1. SPOT Image

The SPOT image was acquired the 3rd November 2001 by HRVIR2 on SPOT 4. It was geo-located by SPOT image (SPOTView Basic product). The projection is UTM 20 South, WGS-84 (please, refer to the campaign report for more details: annex or http://www.avignon.inra.fr/valeri). No atmospheric correction was applied to the image since no atmospheric data were available. However, as the SPOT image is used to compute empirical relationships between reflectance and biophysical variable, we can assume that the effect of the atmosphere is the same over the whole 3 x 3 km site. Therefore, it will be taken into account everywhere in the same way.

Figure 1 shows the relationship between Red and near infrared (NIR) SPOT channels: the soil line is marked (bare soil not much represented) and no saturated points are observed.

[1] Lang, A.R.G. and Xiang, Y., 1986. Estimation of leaf area index from transmission of direct sunlight in discontinuous canopies. Agric. For. Meteorol., 37: 229-243.
[2] Annex or http://www.avignon.inra.fr/valeri

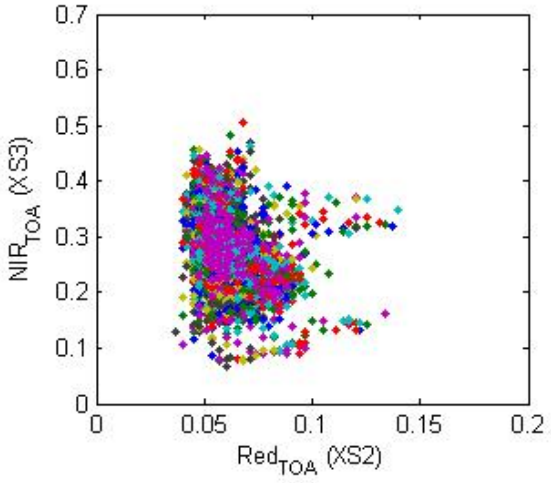

Figure 1. Red/NIR relationship on the SPOT image for Laprida, 2001.

2.2. Hemispherical images

The hemispherical images were processed using the CAN-EYE software (Version 4.2) to derive the biophysical variables. Figure 2 and Figure 3 show the distribution of the several variables over the 37 sampled ESUs. As Laprida is a grassland site, all the hemispherical images were acquired from above the canopy.

Note that LAI (effective and true) derived from directional gap fraction and LAI derived from gap fraction at 57.5° (effective and true) are consistent (Figure 2 and Figure 3). Effective LAI (LAIeff, LAI57eff) varies from 1.01 to 8.36, while true LAI (LAItrue, LAI57true) varies from 1.24 to 10. These ranges show heterogeneous site in terms of LAI. LAIeff and LAI57eff are lower than LAItrue and LAI57true, due to the clumping observed for several ESUs. The relationship between fAPAR and LAI is in agreement with what is expected (Beer-Lambert law) while the fCover-LAI relationship is more noisy (Figure 3).

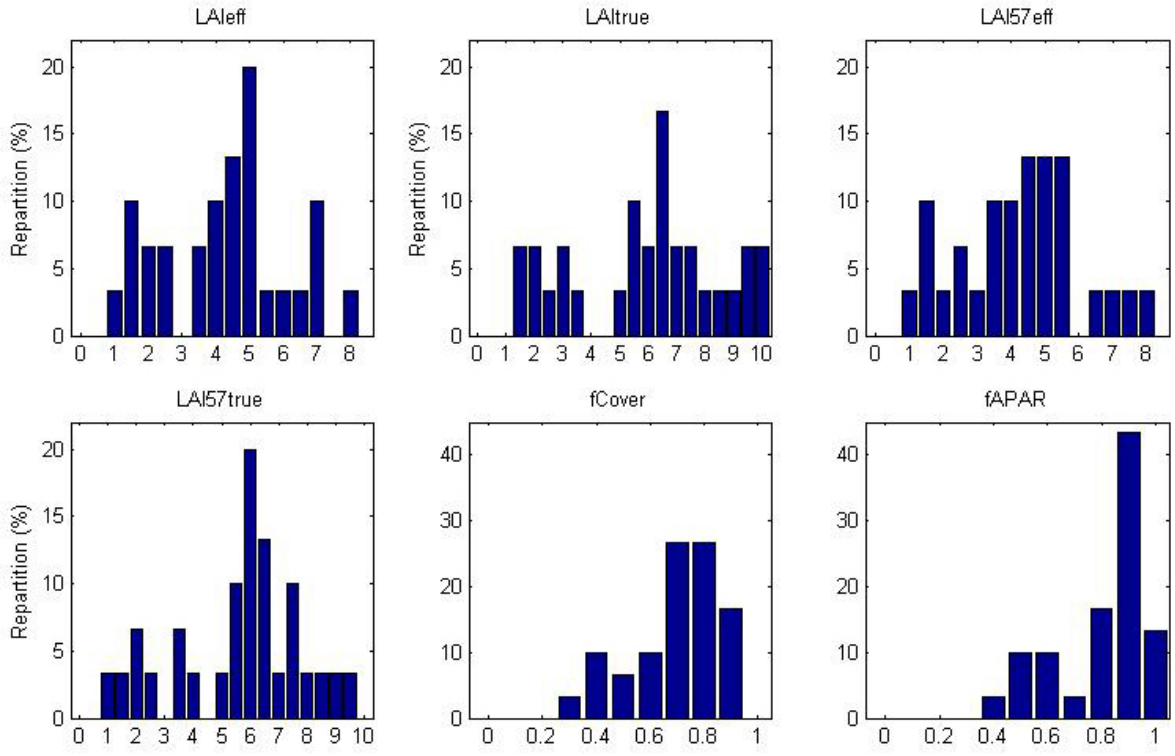

Figure 2. Distribution of the measured biophysical variables over the ESUs.

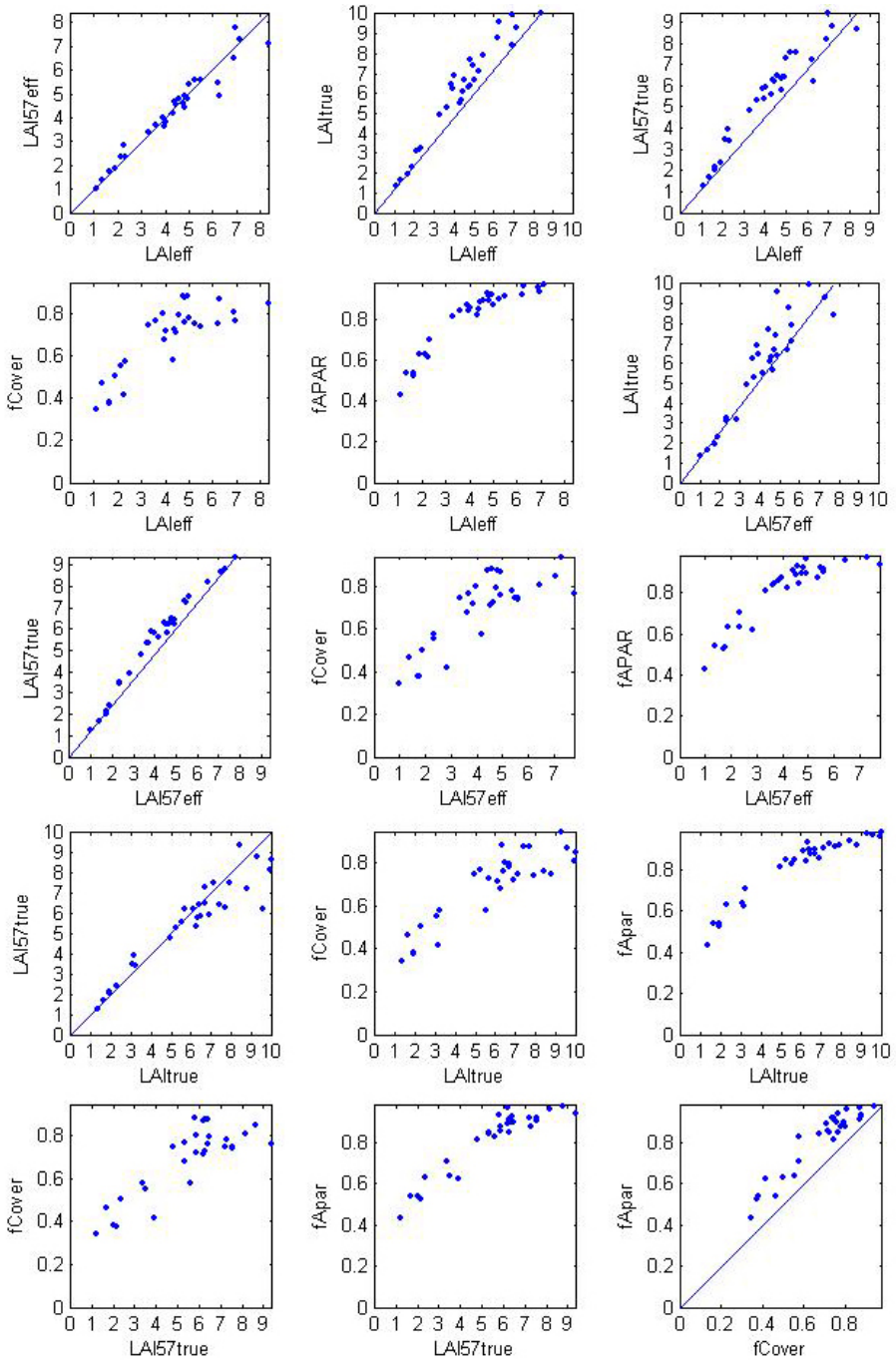

Figure 3. Relationships between the different biophysical variables

2.3. Sampling strategy

2.3.1. Principles

The sampling strategy is defined in the campaign report[3]. The sampling of each ESU is based on six or twelve elementary photographs organized in a cross pattern.

Figure 4 shows that the 37 ESUs are evenly distributed over the site (3 x 3 km). The processing of the ground data has shown that:

- P10, P11, Z9, Z10 and Z11 (in black on Figure 4) were located under a cloud or in the shade;
- Z7 (in black on Figure 4) was located on a small plot with a strong heterogeneity on the borders;

[3] Annex or http://www.avignon.inra.fr/valeri

• for ESU P8, the hemispherical images were very dark (nightfall). We could not use them.

All these ESUs were eliminated. Finally, 30 ESUs have been kept for the computation of the transfer function.

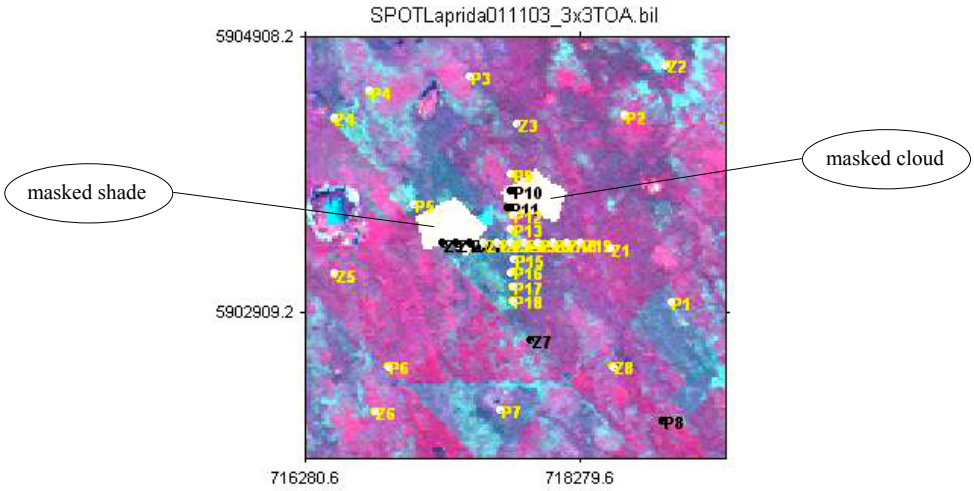

Figure 4. Distribution of the ESUs around the Laprida site. ESUs in black (P8, P10, P11, Z7, Z9, Z10 and Z11) were eliminated for the computation of the transfer function. In white, a mask covering a cloud and its shade.

2.3.2. Evaluation based on NDVI values

The sampling strategy is evaluated using the SPOT image by comparing the NDVI distribution over the site with the NDVI distribution over the ESUs (Figure 5). As the number of pixels is drastically different for the ESUs and whole site (WS = 22500 in case of a 3 x 3 km SPOT image), it is not statistically consistent to directly compare the two NDVI histograms. Therefore, the proposed technique consists in comparing the NDVI cumulative frequency of the two distributions by a Monte-Carlo procedure which aims at comparing the actual frequency to randomly shifted sampling patterns. It consists in:

1. computing the cumulative frequency of the *N* pixel NDVI that correspond to the exact ESU locations;
2. then, applying a unique random translation to the sampling design (modulo the size of the image);
3. computing the cumulative frequency of NDVI on the randomly shifted sampling design;
4. repeating steps 2 and 3, 199 times with 199 different random translation vectors.

This provides a total population of $N = 199 + 1$(actual) cumulative frequency on which a statistical test at acceptance probability $1 - \alpha = 95\%$ is applied: for a given NDVI level, if the actual ESU density function is between two limits defined by the $N\alpha/2 = 5$ highest and lowest values of the 200 cumulative frequencies, the hypothesis assuming that WS and ESU NDVI distributions are equivalent is accepted, otherwise it is rejected.

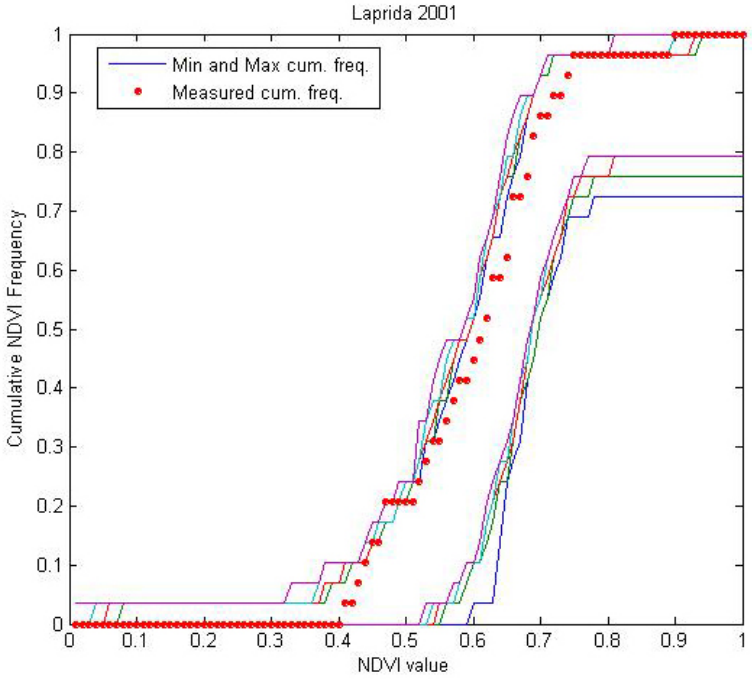

Figure 5. Comparison of the ESU NDVI distribution and the NDVI distribution over the whole image.

Figure 5 shows that the NDVI distribution of the 30 ESUs is good over the whole site (comprised between the 5 highest and lowest cumulative frequencies) even if the cumulative frequency curve reaches the boundaries on several occasions. Note that NDVIs lower than 0.41 have not been sampled either although they are present in the image. They may correspond to surface water, bare soil...

2.3.3. Evaluation based on classification

A non supervised classification based on the k_means method (Matlab statistics toolbox) was applied to the 4 reflectances of the SPOT image to distinguish if different behaviours on the image for the biophysical variable-reflectance relationship exist.

A number of 5 classes was chosen (Figure 6). The distribution of the classes on the image and on the ESUs is different, but each class (except class 2) is represented by at least 4 ESUs. Classes 4 and 5 are under-represented while classes 1 and 3 appear to be over-sampled. Class 2 (in black) corresponds to a cloud and its shade.

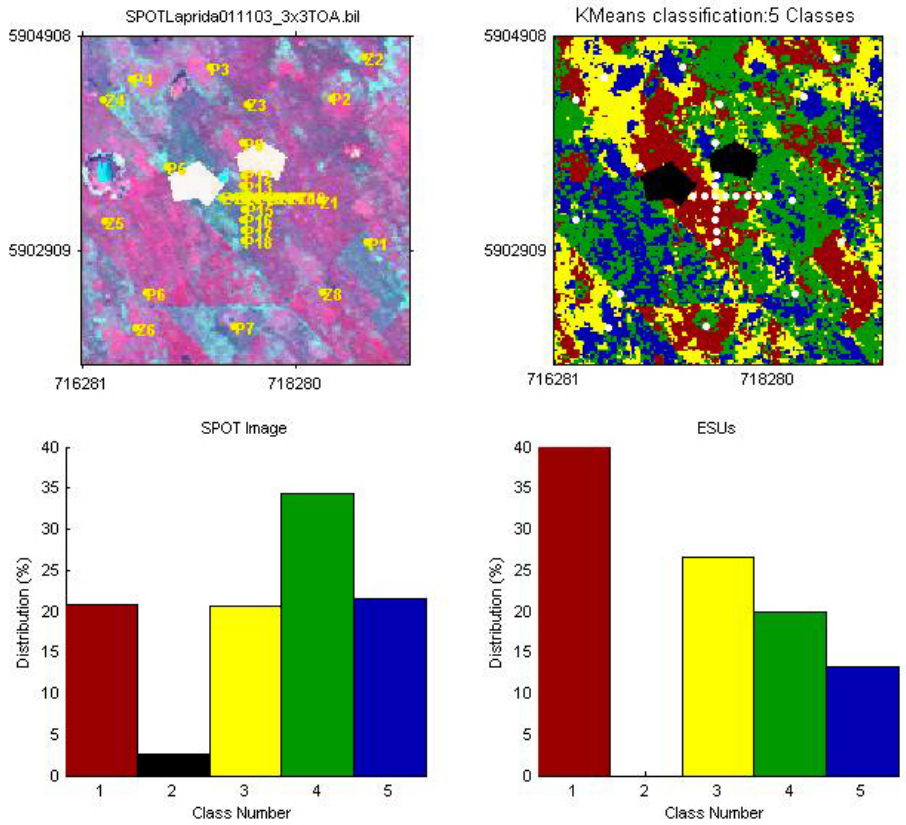

Figure 6. Classification of the SPOT image. Comparison of the class distribution between the SPOT image and sampled ESUs.

Figure 7 shows the different relationships observed between the biophysical variables and the corresponding NDVI on the ESUs, as a function of the SPOT classes determined from non supervised classification.

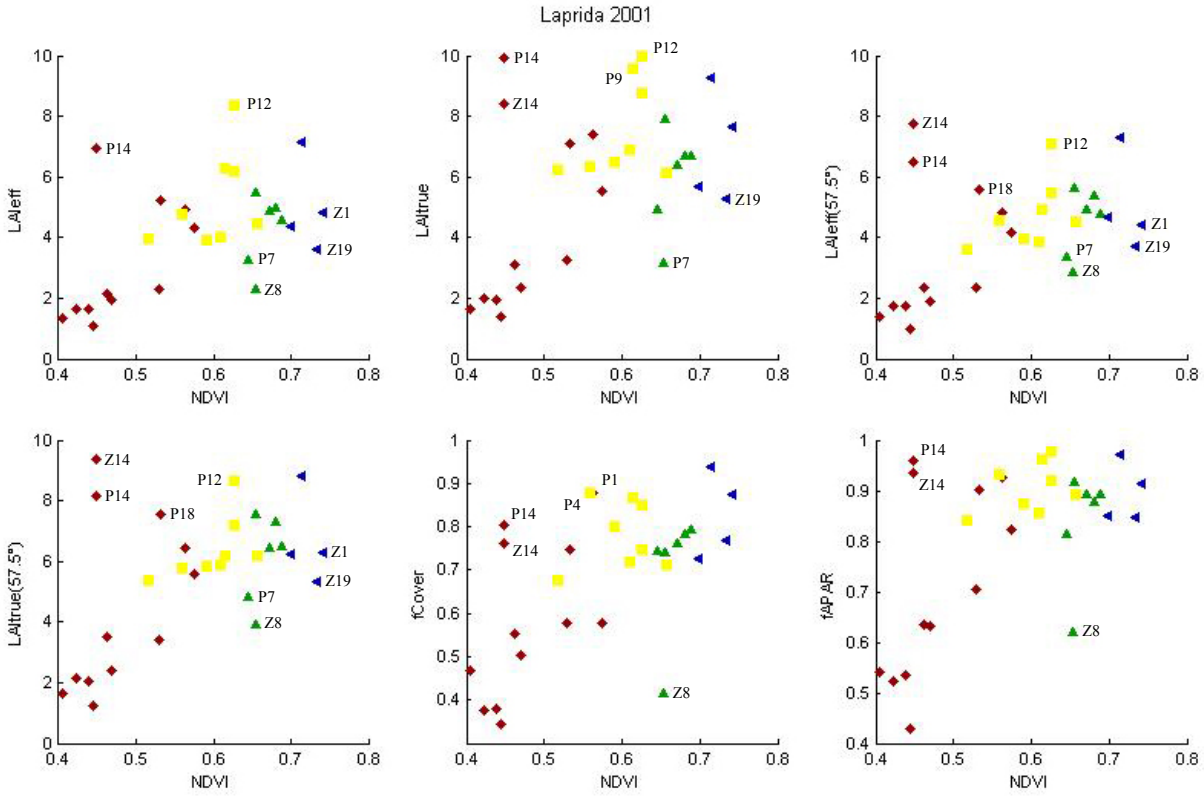

Figure 7. NDVI-Biophysical Variable relationships as a function of SPOT classes

The relation between NDVI and biophysical variables is not very consistent, mainly for a few ESUs (P14, Z14, Z8, Z19…), although a beer-lamber law was expected. Note that the relation is systematically inconsistent for a few ESUs (P14, Z14, Z8, Z19…). This may be due to two features:

1. a presence of water (Z1, P7, Z8 for example). Like in 2002, the campaign took place few days after floodings in the area which modify the reflectance signal and therefore the expected LAI-NDVI relationship (Figure 8);

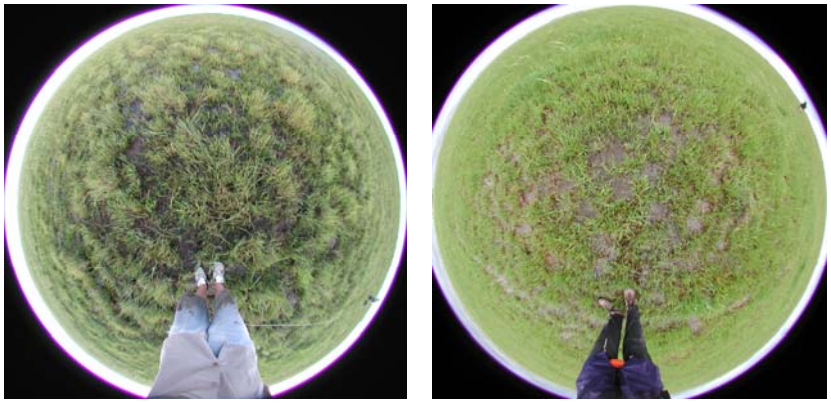

Figure 8. Presence of water on ESUs P7 (left) and Z1 (right).

2. the estimation of the biophysical variables (mainly high LAI values) may not be very accurate since it comes to the limits of the hemispherical images + CAN-EYE processing: as the LAI is quite high and the images are acquired from above the canopy, it is sometimes very difficult to make the difference between the vegetation and the soil when shadows are observed (Figure 9). This distinction is made worse when the soil is covered by water (water is dark, leaves are quite dark and shadowed leaved are very dark).

Figure 9. The difficult to make the difference between the vegetation and the soil when shadows are observed (P18 for example)

2.3.4. Using convex hulls

A test based on the convex hulls was also carried out to characterize the representativeness of ESUs. Whereas the evaluation based on NDVI values uses two bands (red and NIR), this test uses the four bands of the SPOT image. A flag image, is computing over the reflectances (Figure 10). The result on convex-hulls can be interpreted as:

- pixels inside the 'strict convex-hull': a convex-hull is computed using all the SPOT reflectance corresponding to the ESUs belonging to the class. These pixels are well represented by the ground sampling and therefore, when applying a transfer function the degree of confidence in the results will be quite high, since the transfer function will be used as an interpolator;
- pixels inside the 'large convex-hull': a convex-hull is computed using all the reflectance combination (±5% in relative value) corresponding to the ESUs. For these pixels, the degree of confidence in the obtained results will be quite good, since the transfer function is used as an extrapolator (but not far from interpolator);
- pixels outside the two convex-hulls: this means that for these pixels, the transfer function will behave as an extrapolator which makes the results less reliable. However, having a priori information on the site may help to evaluate the extrapolation capacities of the transfer function.

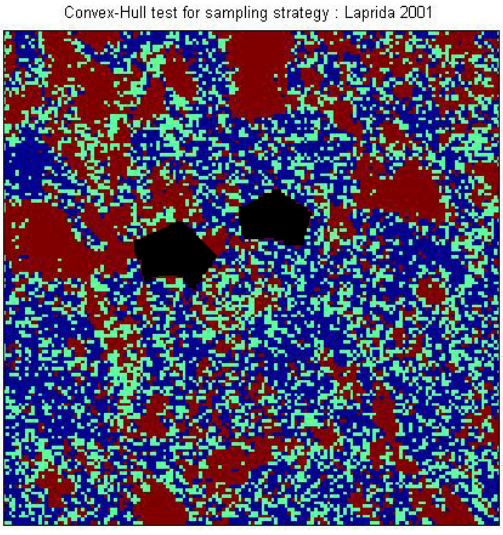

Figure 10. Evaluation of the sampling based on the convex hulls. The map is shown: blue and light blue correspond to the pixels belonging to the 'strict' and 'large' convex hulls and red to the pixels for which the transfer function is extrapolating (in black, the cloud and its shade).

This map shows that the representativeness of the ESUs is good, even if pixels are outside the two convex-hulls. They correspond to surface water, bare soil, high NDVI areas… Note that the areas where the NDVI values are high and the surface is covered by water represent the main part of extrapolated pixels.

3. Determination of the transfer function for the 6 biophysical variables: LAIeff, LAItrue, LAI57eff, LAI57true, fCover, fAPAR

3.1. The transfer functions considered

Two types of transfer functions are usually tested in the frame of the VALERI project:

- AVE: if the number of ESUs belonging to the class is too low. The transfer function consists only in attributing the average value of the biophysical variable measured on the class to each pixel of the SPOT image belonging to the class;

- REG: if the number of ESUs is sufficient, multiple robust regression between ESUs reflectance (or Simple Ratio) and the considered biophysical variable can be applied: we used the 'robustfit' function from the matlab statistics toolbox. It uses an iteratively re-weighted least squares algorithm, with the weights at each iteration computed by applying the bisquare function to the residuals from the previous iteration. This algorithm provides lower weight to ESUs that do not fit well. The results are less sensitive to outliers in the data as compared with ordinary least squares regression. At the end of the processing, three errors are computed: classical root mean square error (RMSE), weighted RMSE (using the weights attributed to each ESU) and cross-validation RMSE (leave-one-out method).

Even if the relationship between NDVI and LAI (§2.3.3) is not very consistent, the 'REG' method is applied since the results are rather pertinent.

3.2. Results

3.2.1. Choice of the method

For all the ESUs, a single transfer function was computed. Figure 11 shows the results obtained for all the possible band combinations using either the reflectance (ρ) or the logarithm of the reflectance (log(ρ)). Even if the regression made on the log(ρ) provides slightly better results (LAItrue, fCover and fAPAR), the results using the reflectance (ρ) were selected for all the variables. For these variables, the transfer function using the log(ρ) creates coplanar points which do not allow the determination of the 'strict' and 'large' convex hulls.

Note that the Red*NIR ('+' or RN) combination is added to all the band combinations (except for NDVI and SR). Please read the document: "a method to improve the relation between the biophysical variables" (http://www.avignon.inra.fr/valeri/table_methods/new_linear.pdf).

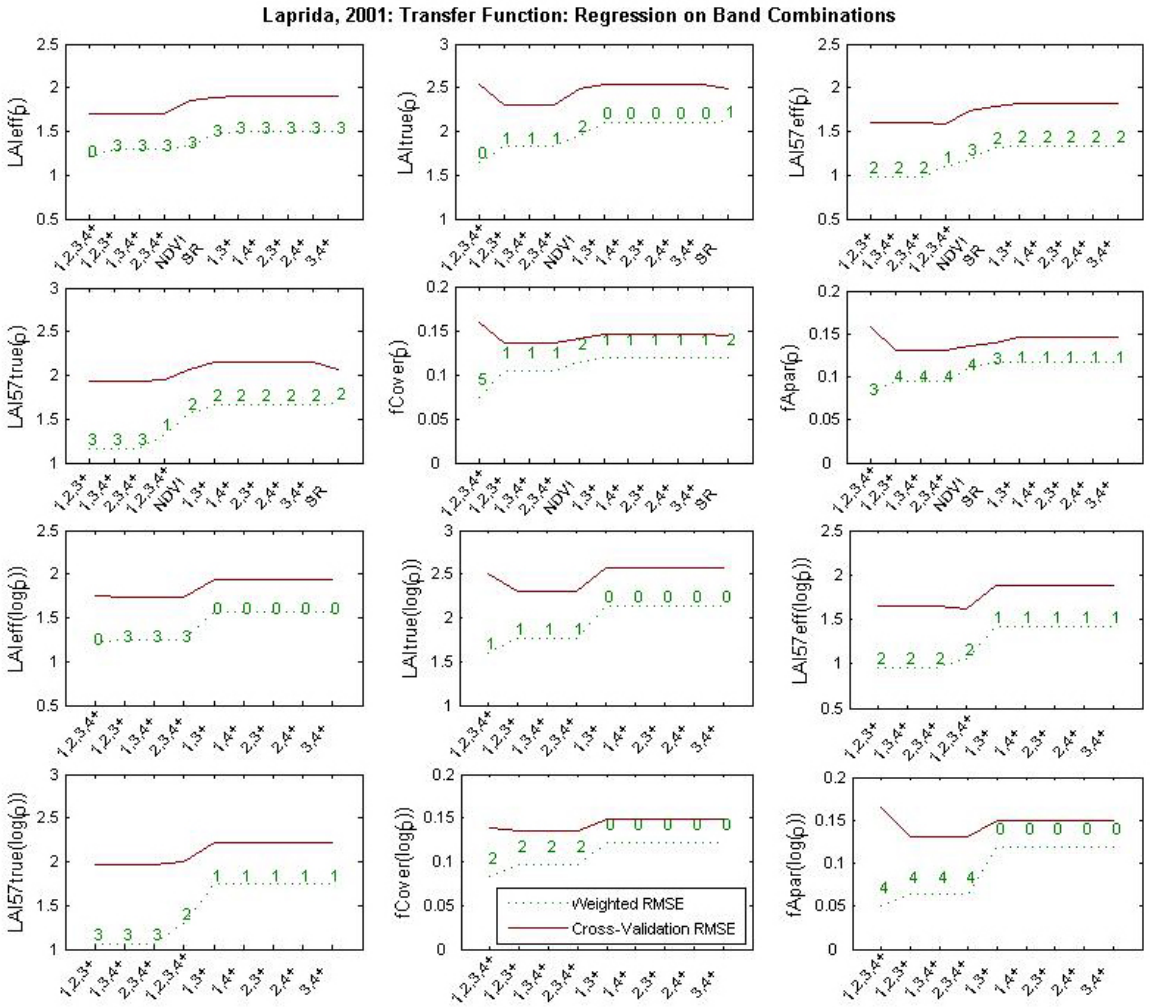

Figure 11. Transfer function: test of multiple regression applied on different band combinations. Band combinations are given in abscissa. The estimated biophysical variable is given in ordinate. Top graphs correspond to regression made on reflectance (ρ): the weighted root mean square error (RMSE) is presented in green along with the cross-validation RMSE in red. The numbers indicate the number of data used for the robust regression with a weight lower than 0.7 that could be considered as outliers. Bottom graphs correspond to regression made on the logarithm of the reflectance.

3.2.2. Choice of the band combination

For the LAIeff, the XS1, XS2, XS3, XS4, RN (Figure 12 and Figure 13) combination on reflectance was selected since it provides a good compromise between the cross-validation RMSE (among the lowest values), the weighted root mean square error (lowest value) and the RMSE (lowest value). Note that no weight is lower than 0.7.

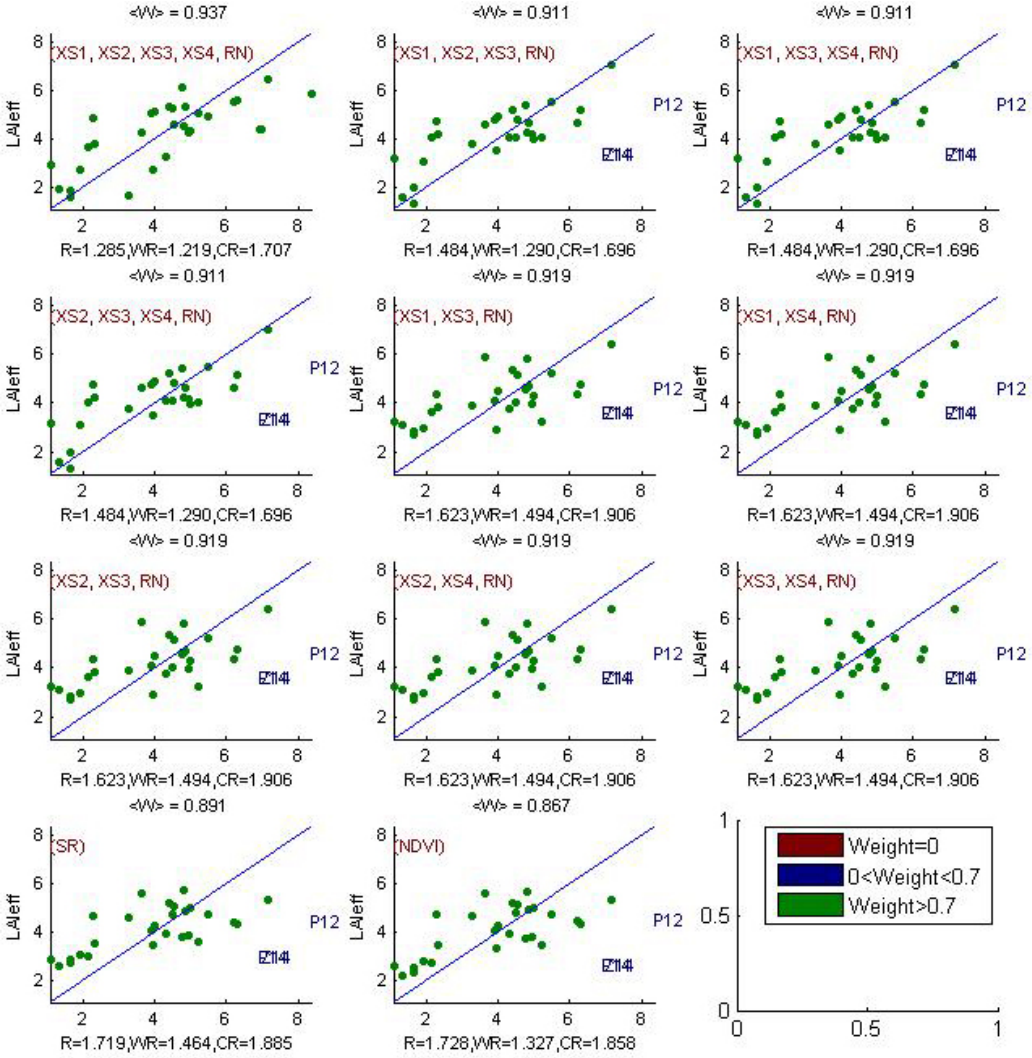

Figure 12. Effective Leaf Area Index: results for regression on reflectance using different band combinations. R is the root mean square error computed between LAIeff and estimated LAIeff. WR is the weighted root mean square error and CR is the cross validation root mean square error.

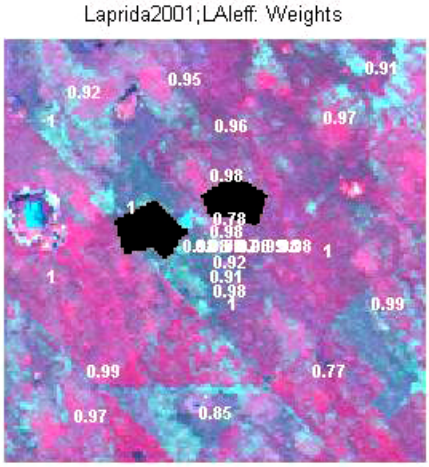

Figure 13. Weights associated to each ESU for the determination of LAIeff transfer function.

For the LAItrue, in spite of the cross-validation RMSE value, the XS1, XS2, XS3, XS4, RN (Figure 14 and Figure 15) combination on reflectance was selected since it provides the lowest weighted root mean square error value, the lowest RMSE value and no weight lower than 0.7. Note that the XS1, XS2, XS3, XS4, RN combination on the log(ρ) provides better results, but the transfer function using the log(ρ) creates coplanar points which do not allow the determination of the 'strict' and 'large' convex hulls.

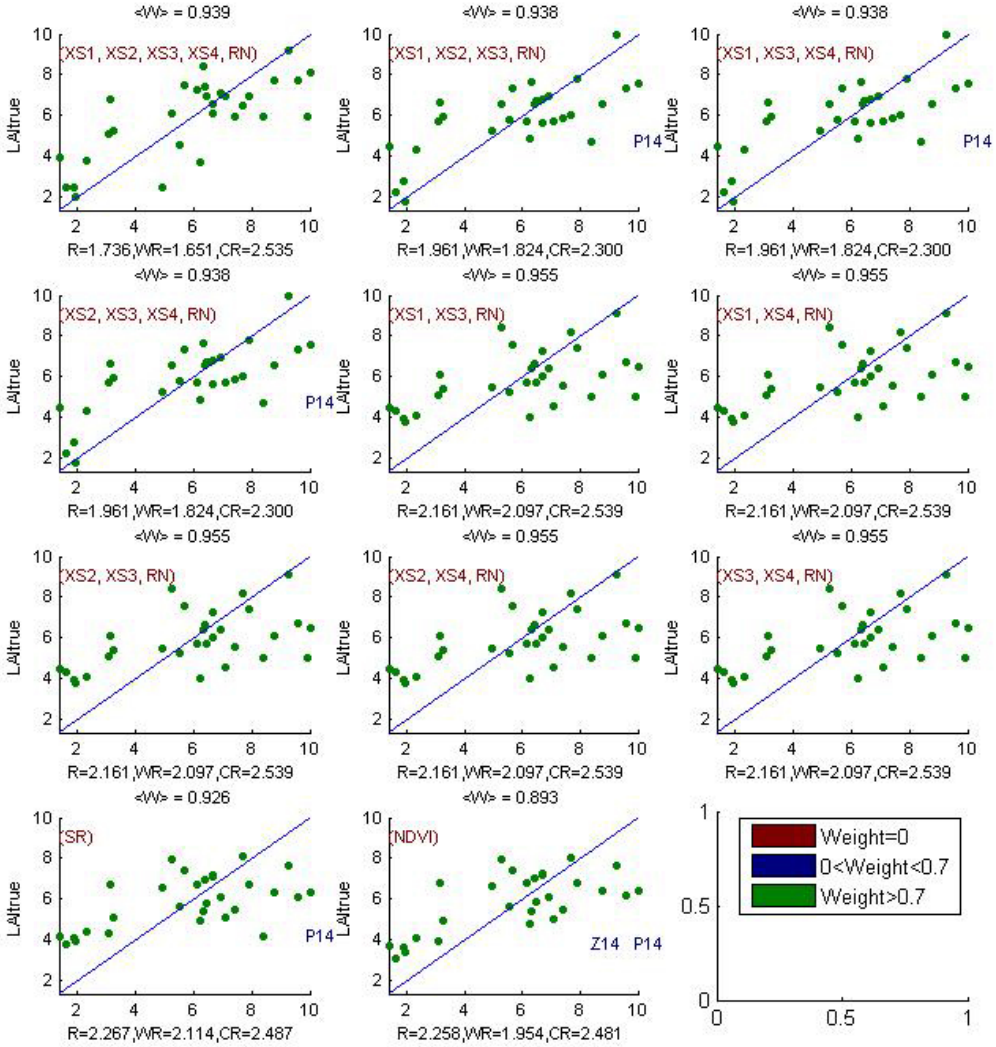

Figure 14. True Leaf Area Index: results for regression on reflectance using different band combinations. R is the root mean square error computed between LAItrue and estimated LAItrue. WR is the weighted root mean square error and CR is the cross validation root mean square error.

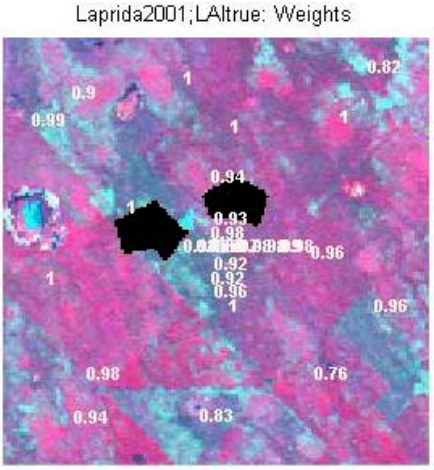

Figure 15. Weights associated to each ESU for the determination of LAItrue transfer function.

For the LAI57eff, the XS1, XS2, XS3, XS4, RN (Figure 16 and Figure 17) combination on reflectance was selected since it provides a good compromise between the cross-validation RMSE (lowest value), the weighted root mean square error and the RMSE (lowest value). Note that one weight is lower than 0.7.

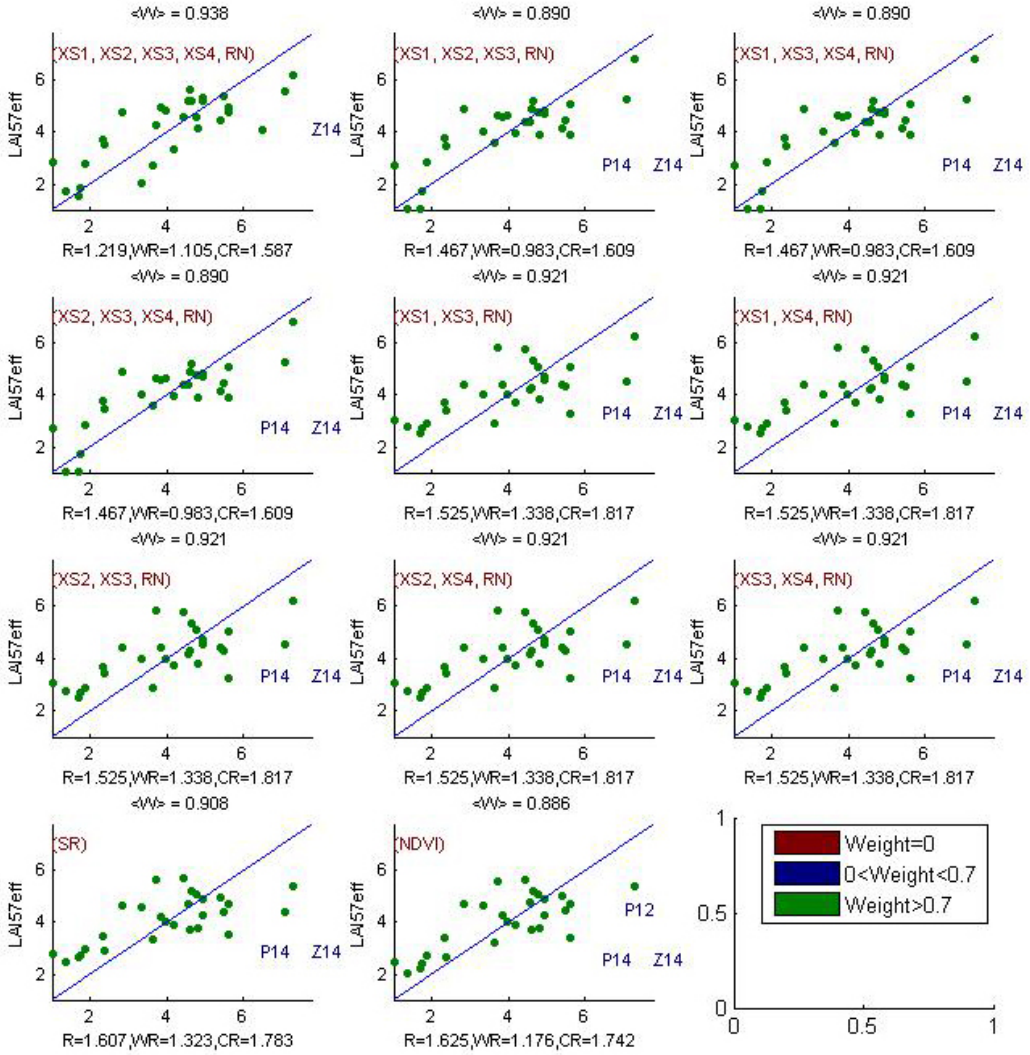

Figure 16. Effective LAI at 57.5°: results for regression on reflectance using different band combinations. R is the root mean square error computed between LAI57eff and estimated LAI57eff. WR is the weighted root mean square error and CR is the cross validation root mean square error.

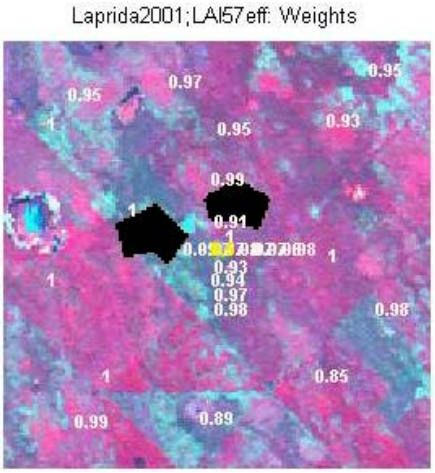

Figure 17. Weights associated to each ESU for the determination of LAI57eff transfer function.

For the LAI57true, the XS1, XS2, XS3, XS4, RN (Figure 18 and Figure 19) combination on reflectance was selected since it provides a good compromise between the cross-validation RMSE (among the lowest values), the weighted root mean square error and the RMSE (lowest value). Note that one weight is lower than 0.7.

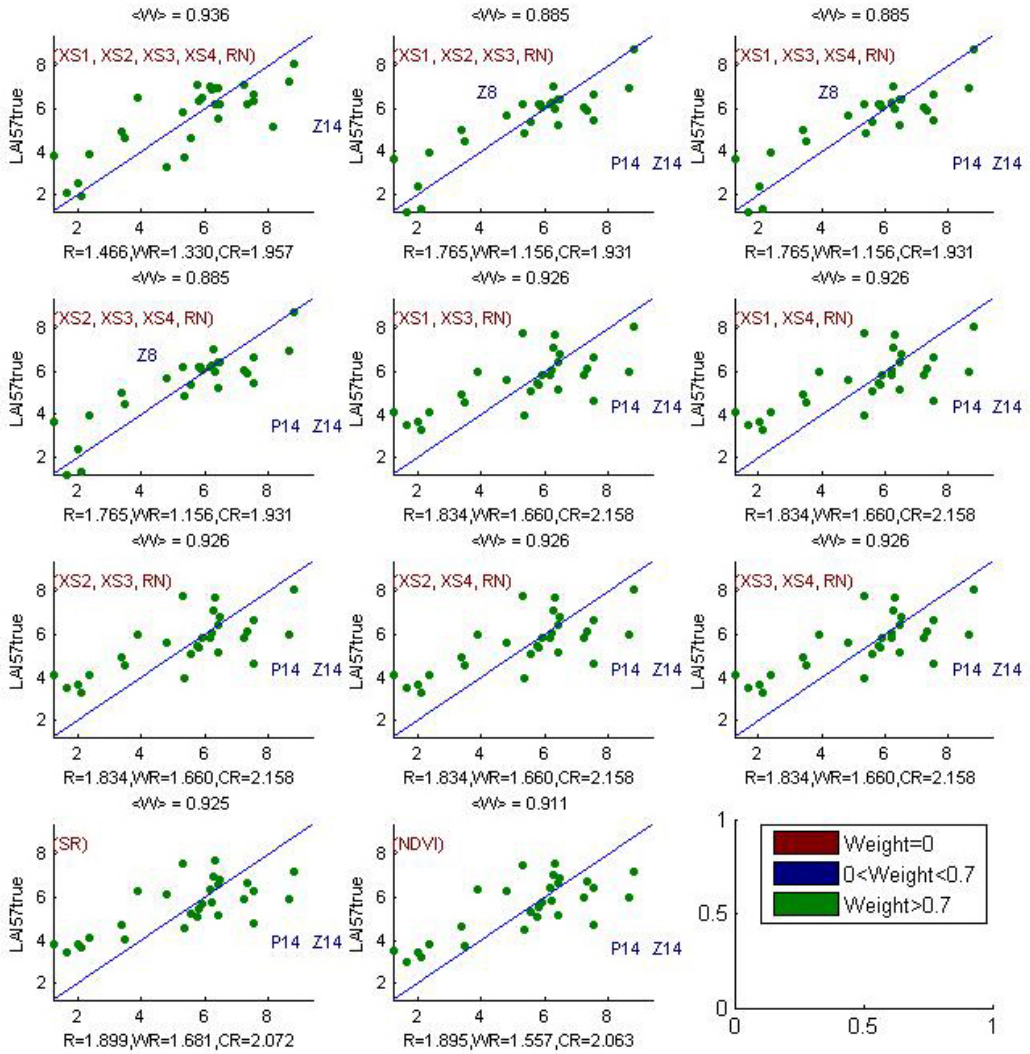

Figure 18. True Leaf Area Index at 57.5°: results for regression on reflectance using different band combinations. R is the root mean square error computed between LAI57true and estimated LAI57true. WR is the weighted root mean square error and CR is the cross validation root mean square error.

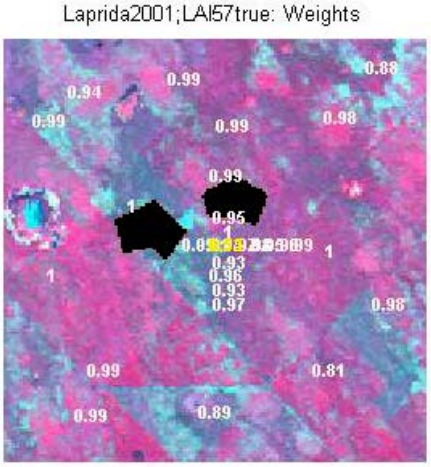

Figure 19. Weights associated to each ESU for the determination of LAI57true transfer function.

For the fCover, the XS2, XS3, XS4, RN (Figure 20 and Figure 21) combination on reflectance was selected since it provides a good compromise between the cross-validation RMSE (among the lowest values), the weighted root mean square error and the RMSE (among the lowest values). Two weights are lower than 0.7. Note that the XS1, XS2, XS3, XS4, RN combination on the log(ρ) provides better results, but the transfer function using the log(ρ) creates coplanar points which do not allow the determination of the 'strict' and 'large' convex hulls.

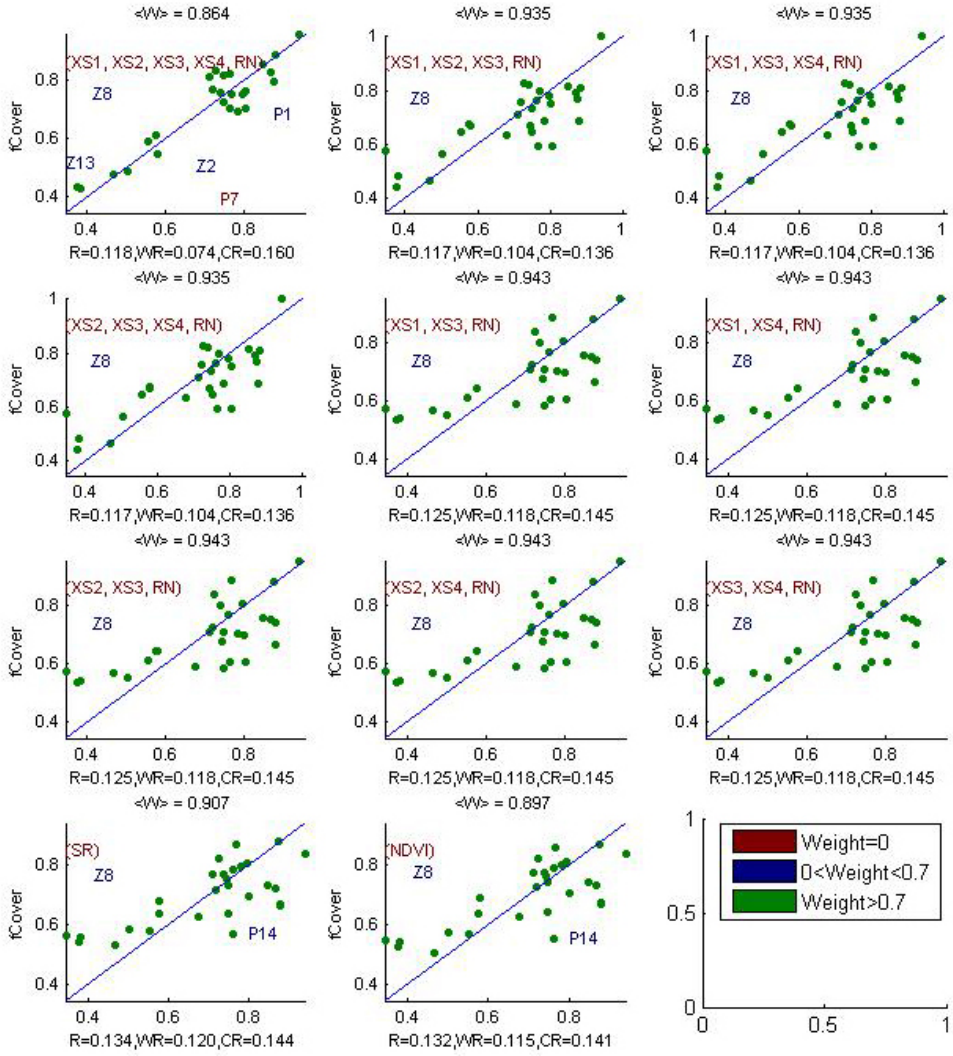

Figure 20. fCover: results for regression on reflectance using different band combinations. R is the root mean square error computed between fCover and estimated fCover. WR is the weighted root mean square error and CR is the cross validation root mean square error.

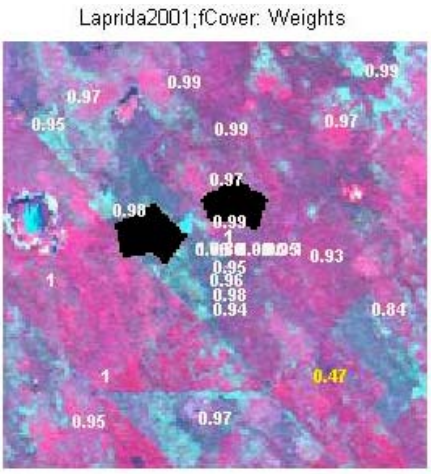

Figure 21. Weights associated to each ESU for the determination of fCover transfer function.

For the fAPAR, the XS2, XS3, XS4, RN (Figure 22 and Figure 23) combination on reflectance was selected since it provides a good compromise between the cross-validation RMSE (lowest value), the weighted root mean square error and the RMSE. Four weights are lower than 0.7. Note that the XS2, XS3, XS4, RN combination on the log(ρ) provides better results (mainly WR), but the transfer function using the log(ρ) creates coplanar points which do not allow the determination of the 'strict' and 'large' convex hulls.

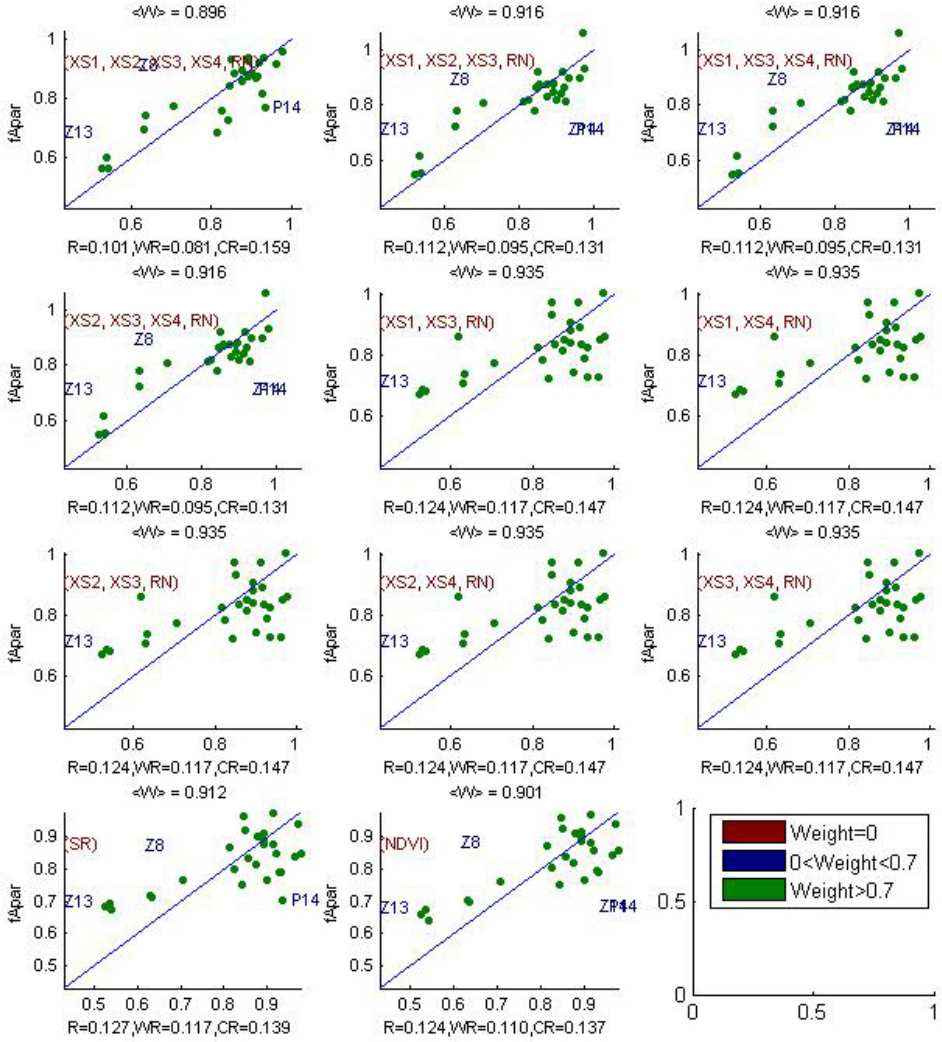

Figure 22. fAPAR: results for regression on reflectance using different band combinations. R is the root mean square error computed between fAPAR and estimated fAPAR. WR is the weighted root mean square error and CR is the cross validation root mean square error.

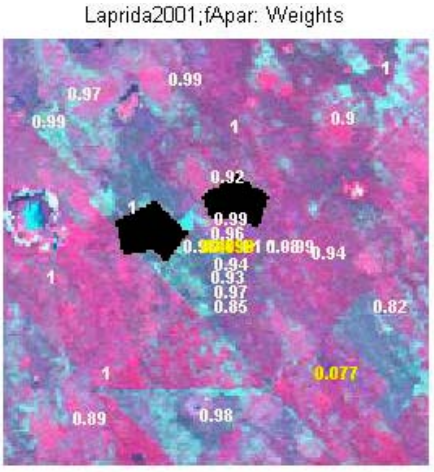

Figure 23. Weights associated to each ESU for the determination of fAPAR transfer function.

Following, the results of the transfer function (Table 2):

Variable	Band Combination	RMSE	Weighted RMSE	Cross-valid RMSE
LAIeff	45.887 - 228.01(XS1) - 558.69(XS2) - 124.63(XS3) + 50.329(XS4) + 2339.5(RN)	1.285	1.219	1.707
LAItrue	63.926 - 315.53(XS1) - 777.04(XS2) - 171.84(XS3) + 65.563(XS4) + 3258(RN)	1.736	1.651	2.535
LAI57eff	41.259 - 183.19(XS1) - 522.33(XS2) - 111.56(XS3) + 43.73(XS4) + 2093.5(RN)	1.219	1.105	1.587
LAI57true	51.587 - 190.57(XS1) - 689.77(XS2) - 141.09(XS3) + 51.825(XS4) + 2631.7(RN)	1.466	1.330	1.957
fCover	3.8406 - 18.625(XS2) - 37.25(XS3) - 9.0532(XS4) + 195.62(RN)	0.117	0.104	0.136
fAPAR	4.1209 - 12.524(XS2) - 45.531(XS3) - 10.594(XS4) + 210.31(RN)	0.112	0.095	0.131

RN = Red*NIR

Table 2. Transfer function applied to the whole site for the different biophysical variables, and corresponding errors

3.3. Applying the transfer function to the Laprida SPOT image extraction

Figure 24 presents the biophysical variable maps obtained with the transfer function described in Table 2 for the classes 1, 3, 4 and 5 (class 2 corresponds to the cloud and the shade). The maps obtained for the six variables are consistent, showing similar patterns: low LAIeff values where low fCover or fAPAR are observed and conversely… As the NDVI values corresponding to ground measurements on the Laprida site were between 0.40 and 0.74, the multi-linear regression is valid only for NDVI ranging between these two values. The extrapolation capacity of this relationship may not be good in certain conditions. Indeed, when applying the relationship on a few pixels in the image (at the scale of the site: 23 pixels (0.09%) for LAIeff; 88 pixels (0.38%) for LAItrue; 9 pixels (0.03%) for LAI57eff; 28 pixels (0.12%) for LAItrue), the regression provides unrealistic results such as extremely high (up to 25) values of LAI. We have no indication in the image and no knowledge of the ground cover which could explain bad regression results. However, as these pixels correspond to high NDVI values, the maximum measured LAI was attributed (effective LAI = 8,4; true LAI = 10).

The difference between effective LAI and true LAI is significant (see the average values in Figure 24). This was expected when looking the LAIeff/LAItrue relationship, showing that for high LAI the difference between the two can be significant.

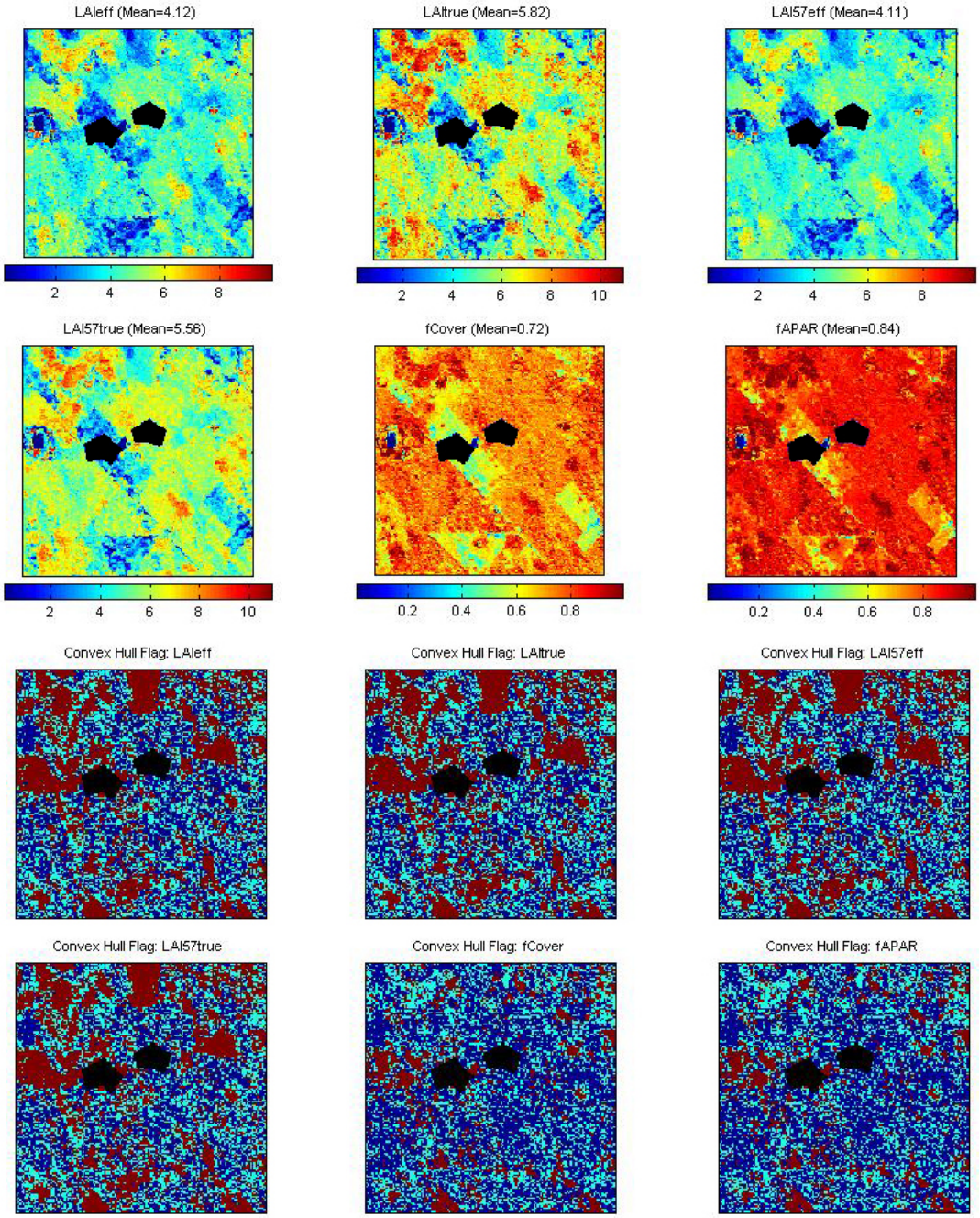

Figure 24. High resolution biophysical variable maps applied on the Laprida site (top). Associated Flags are shown: blue and light blue correspond to the pixels belonging to the 'strict' and 'large' convex hulls, red to the pixels for which the transfer function is extrapolating. In black, the cloud and its shade (mask).

The flag maps are comparable between LAIeff, LAItrue, LAI57eff and LAI57true, and between fCover and fAPAR. The extrapolation mainly corresponds to surface water, bare soil, mixed pixels, high LAI areas (§2.3.2)… The pixels inside the strict convex hull for are more numerous in the fCover and fAPAR maps. This is due to the choice of the band combination.

4. Conclusion

The transfer function is obtained by using 30 ESUs. The Laprida site is quite heterogeneous in terms of LAI and NDVI. The relationship between these two variables is not very consistent, but the representativeness of the

ESUs is good and the transfer function is used as an extrapolator in little areas. The site is particular since there is a strong presence of surface water. Note that the number and the place of sensor spectral bands do not make it possible to take into account the presence of water correctly. Therefore, the estimation of LAI from the 4 bands is more uncertainly. Moreover the estimation of biophysical variables above grassland with surface water or shadows as well as for high LAIs is more difficult with the CAN-EYE software. However, the results of the robust regression are rather satisfactory and the maps obtained for the biophysical variables are consistent. The flag associated to each map show that the extrapolation is mainly related to the presence of surface water, bare soil, high LAI areas… For all the variables, the regression coefficients are computed by relating the variable itself to reflectance (§3.2.1).

The biophysical variable maps are available in UTM, 20 South, projection coordinates (Datum: WGS-84) at 20 m resolution.

5. Acknowledgements

We thank people who participated to the field experiment: **Mario Carpi** (Farm owner) and **Ricardo Castex** (Farm manager), **Marie Weiss** (Noveltis/INRA CSE), **Vicky Feler**, **Frederico Bock** and **Carlos Di Bella** (INTA, Instituto de Climat y Agua).

ANNEX

Ground measurement acquisition report for the VALERI site **Laprida**

from 5th November 2001 to 8th November 2001

Carlos Di Bella/Marie Weiss
Organization: INTA/Noveltis, INRA CSE
email: marie.weiss@avignon.inra.fr

Date of report: 19/08/03

People participating to the field experiment:

Fistname & Name	0rganization
Weiss Marie	Noveltis/INRA CSE
Di Bella Carlos	INTA, Instituto de Climat y Agua
V. Feler	INTA, Instituto de Climat y Agua
F. Bock	INTA, Instituto de Climat y Agua

Site coordinates

	Lat-Long WGS84 (Deg min.00)		**UTM / WGS84** UTM 20S	
	Lat.	Lon.	Easting	Northing
Upper left corner	-36.977094	-60.57017	5904909.2	716279.6
Lower right corner	-37.003594	-60.535392	5901889.2	719299.6

Ground control points

# Name	Day	Month	Easting(m)	Northing(m)
GCP1	9	11	699198	5896453
GCP2	9	11	755387	5918801
GCP3	9	11	751742	5879505
GCP4	9	11	731971	5901374
GCP5	9	11	735031	5911873
GCP6	9	11	698802	5894391
GCP7	9	11	711270	5903763
GCP8	9	11	684792	5927962

GPS system used: Garmin.

Description of the site and land cover

Category according to IGBP classification

Grassland.

Comments on the land cover

Native and successional grasslands in both Flooding and Southern Pampa are characterised by the co-dominance of C3 and C4 grasses. Aboveground net primary 127 production of these grasslands range between 4500 and 5500 kg m -2 y -1. The climate is humid temperate, with a mean annual precipitation 129 between 700 and 800 mm y -1 and mean annual temperature of 14°C. Perennial pastures, used for cattle grazing of hay production, are very extensive in the area. They are often composed by alfalfa alone or alfalfa plus some C3 grass like Bromus unioloides or Dactylis glomerata. Pastures are generally part of the crop rotation system. They are used during 3 to 6 years and then the paddock is used for annual crops again. Where soil conditions are not appropriate for cropping, it is frequent that native grasslands are inter-sowed with Agropyron sp. or Festuca arundinacea[4].

Topography

Altitude ≈ 200m.

[4] Guerschman, JP; Paruelo, JM; Di Bella, CM; Giallorenzi, MC and Pacin, F (2001): Land Cover Classification in Argentine Pampas using multitemporal landsat TM data. **International Journal of Remote Sensing (Accepted)**

Land cover map

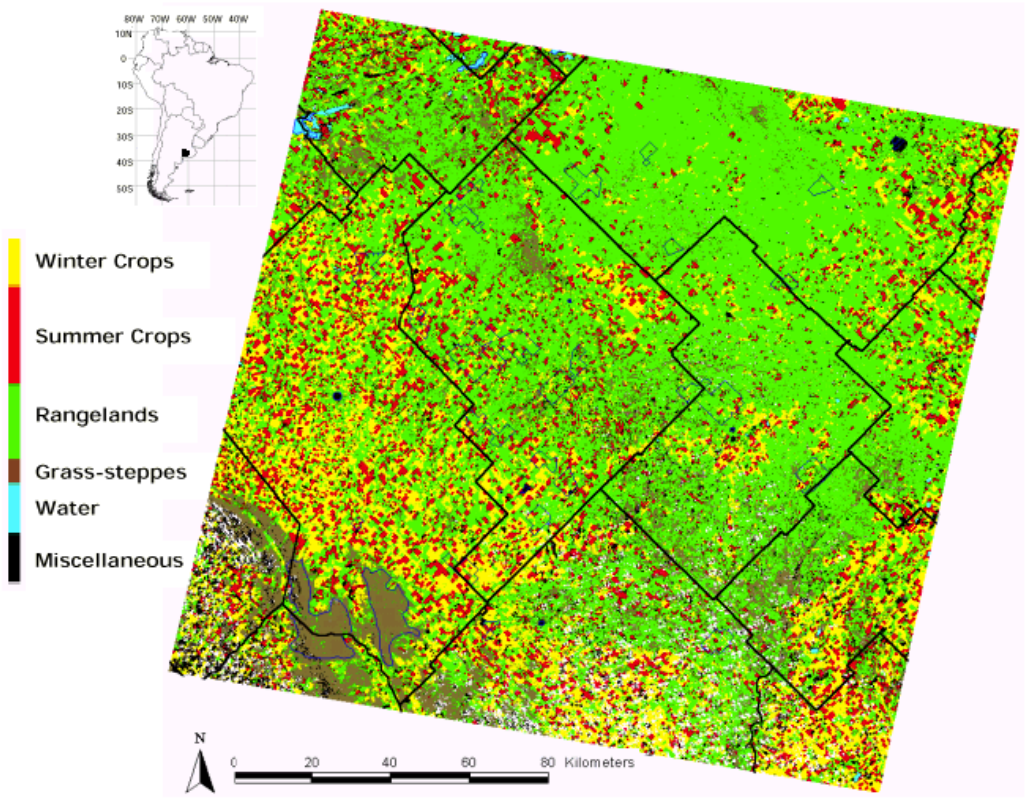

Spatial Sampling scheme

Sensors used for sampling the ESUs

	Method	Comments
☒	Hemispherical photographs	
☐	LAI2000	
☐	TRAC	
☐	Ceptometer	
☐	Direct measurements	
☐	Other	

Sampling strategy for the ESU

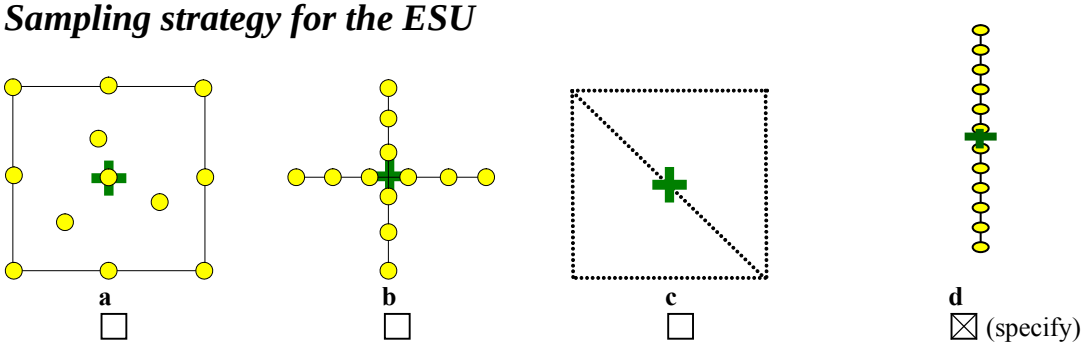

Distribution of the Elementary sampling units

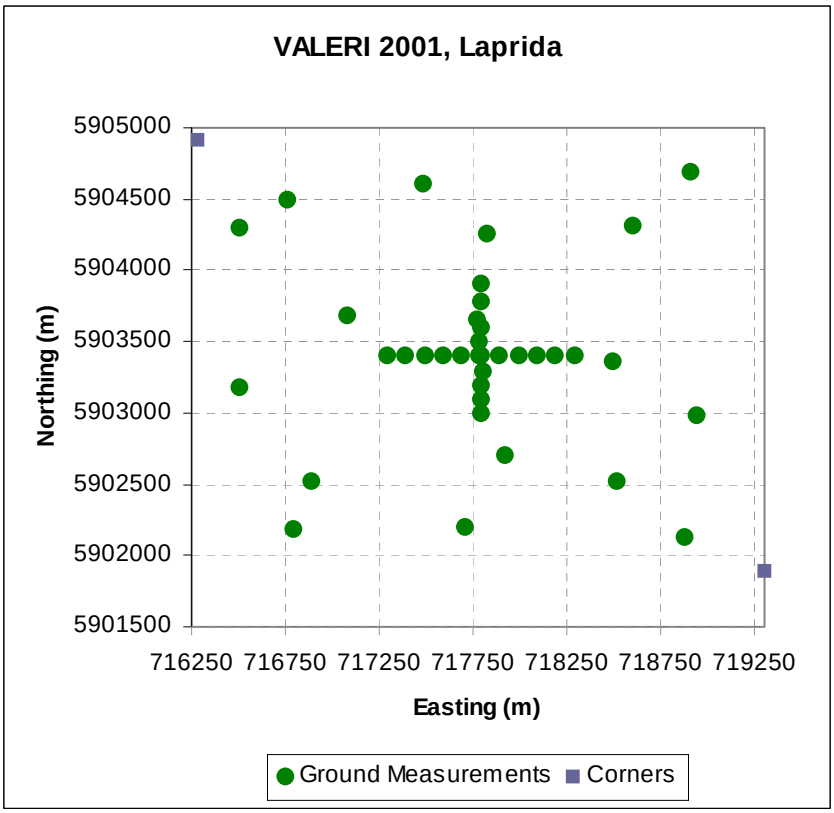

The high spatial resolution image

Satellite

Satellite used	SPOT4 HRV2
Level of processing	2B
Projection type	UTM, WGS84, 20S
Date	3rd November 2001

List of the ESUs

# Name	Day	Month	Easting(m)	Northing(m)
GCP1	9	11	699198	5896453
GCP2	9	11	755387	5918801
GCP3	9	11	751742	5879505
GCP4	9	11	731971	5901374
GCP5	9	11	735031	5911873
GCP6	9	11	698802	5894391
GCP7	9	11	711270	5903763
GCP8	9	11	684792	5927962
ULC			716279	5904909
LRC			719299	5901889
Z1	5	11	718491	5903368
Z2	6	11	718903	5904699
P1	5	11	718936	5902984
P2	5	11	718597	5904320
Z3	6	11	717821	5904264
Z4	6	11	716500	5904306
Z5	6	11	716505	5903180
Z6	6	11	716792	5902193
Z7	6	11	717922	5902706
Z8	6	11	718517	5902519
P3	6	11	717479	5904603
P4	6	11	716756	5904500
P5	6	11	717079	5903683
P6	6	11	716892	5902518
P7	6	11	717704	5902202
P8	6	11	718876	5902128
Z9	7	11	717289	5903401
Z10	7	11	717389	5903401
Z11	7	11	717489	5903401
Z12	7	11	717589	5903401
Z13	7	11	717689	5903401
Z14	7	11	717789	5903401
Z15	7	11	717889	5903401
Z16	7	11	717989	5903401
Z17	7	11	718089	5903401
Z18	7	11	718189	5903401
Z19	7	11	718289	5903401
P9	7	11	717788	5903902
P10	7	11	717788	5903785
P11	7	11	717769	5903663
P12	7	11	717792	5903607
P13	7	11	717785	5903504
P14	7	11	717784	5903403
P15	7	11	717797	5903291
P16	7	11	717787	5903199
P17	7	11	717790	5903095
P18	7	11	717790	5902997

Acknowledgements

We want to thank Mr. Mario Carpi and Ricardo Castex (owner and manager of the farm, respectively) for the invaluable help in the measurements.

Gauchos and cows

Carlos Vicky

Frederico